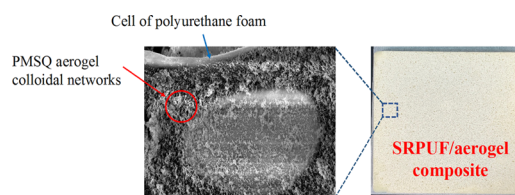# Semi-Rigid Polyurethane Foam and Polymethylsilsesquioxane Aerogel Composite for Thermal Insulation and Sound Absorption

Byeong Seok Kim
Jinkyu Choi
Ye Seo Park
Yingjie Qian
Sang Eun Shim*

Department of Chemistry and Chemical Engineering, Education and Research Center for Smart Energy and Materials, Inha University, Incheon 22212, Korea

Abstract: Although aerogels exhibit excellent thermal insulating properties, their high costs and poor mechanical properties have hindered their application. Semi-rigid polyurethane foams (SRPUFs) have been widely used in daily life as thermal and acoustic insulators owing to their low cost and good mechanical properties despite their poorer thermal insulating performance compared with aerogels. To utilize both aerogels and SRPUFs, in this study, we prepared a SRPUF/aerogel composite using an economical and practical approach for the first time. Specifically, a sol state of polymethylsilsesquioxane (PMSQ) was prepared via the hydrolysis of methyltrimethoxysilane under acidic conditions, followed by the gelation of PMSQ on the surface of SRPUF under basic conditions to yield the SRPUF/aerogl composite. The fabricated SRPUF/aerogel composite with 63 phr (parts per hundred resin) of PMSQ aerogel exhibits promising properties, including a decline in the thermal conductivity from 41.0 to 36.0 mW/m·K and an improvement in the average sound absorption coefficient at higher frequency range from 0.57 to 0.67 compared with neat SRPUF. Moreover, the composite exhibits enhanced hydrophobicity, which is crucial for preserving the structural, thermal, and acoustic features of the composite in use. Hence, we expect that this study will set a precedent for the utilization of the excellent thermal properties of aerogels for various applications.

Keywords: semi-rigid polyurethane, polymethylsilsesquioxane aerogel, fluoric surfactant, thermal insulation.

Cell of polyurethane foam

PMSQ aerogel colloidal networks

SRPUF/aerogel composite

1. Introduction

Considerable amount of energy is wastefully dissipated while controlling the temperature in buildings, maintaining the temperature of automobile engines, and operating plants. Therefore, developing thermal insulating materials is an essential undertaking.[1-5] Owing to their low thermal conductivity, polyurethane foams (PUFs) have been widely used as thermal insulating materials in buildings, ships, cars, and pipes.[6,7] PUFs are also used for reducing sound/noise, vibration, and absorbing energy.[7,8] Generally, PUFs can be classified into three types: rigid, flexible, and semi-rigid.[9] PUFs with flexible mechanical properties are mostly composed of open cells and are referred to as flexible PUFs (FPUFs). Consequently, FPUFs are mainly used for cushioning, sound absorption, and vibration damping, such as in shoes, furniture, and automotives.[7,10,11] PUFs with rigid mechanical properties, composed of closed cells with insulating gas inside, are referred to as rigid PUFs (RPUFs). RPUFs have been widely used as thermal insulators.[12-14] PUFs having intermediate properties between FPUFs and RPUFs are referred to as semi-rigid PUFs (SRPUFs).[7] SRPUFs exhibit lower thermal conductivities

than FPUFs and higher flexibility than RPUFs. Hence, SRPUFs are promising materials for overcoming the inherent shortcoming of RPUFs as thermal insulators, namely, excess plasticity, which is likely to induce structural deformation and result in a lower sound absorption coefficient.

Silica aerogels, which are mesoporous materials synthesized by the sol-gel process, display unique chemical and physical properties. They have incredibly high porosities (>90%), high specific surface area (500-1200 m^2/g), extremely low bulk densities (<0.1 g/cm^3), tiny pores (<50 nm), and extremely low thermal conductivities (<15 mW/m·K).[15-17] Given these properties, the application of silica aerogels in thermal insulators,[18] supercapacitors,[19] catalyst supports,[20] and low-*k* materials has been widely studied.[21] However, unlike PUFs, aerogels are not commercially used because aerogels are too fragile for industrial purposes, and the cost of synthesizing aerogels is also higher than that of other commercialized thermal insulating materials as a tedious and costly supercritical drying process is required.[16] To overcome these obstacles hindering practical applications of silica-based aerogels, various strategies have been proposed to strengthen the skeletal structures of the aerogels by ageing,[22] crosslinking chemically with organic polymers,[23-25] drying under ambient pressure,[26,27] and hydrophobic surface modification.[28] Although these strategies lead to a evident enhancement of the mechanical strength of aerogels, they suffer from some shortcomings such as increases in the density and thermal conductivity and a decrease in the transparency. Recently, Kanamori *et al.* prepared flexible and transparent aerogels using the trifunctional silane precursor

methyltrimethoxysilane (MTMS) instead of the prevailing precursor (tetraalkoxylsilane) by a simple one-step process without sacrificing the transparency, density, or thermal insulating properties.[29] These aerogels are flexible and can be prepared *via* ambient pressure drying. Furthermore, Kanamori et al. obtained polymethylsilsesquioxane (PMSQ) aerogels by using a suitable surfactant to effectively suppress phase separation during the sol-gel process.[29,30]

To explore the practical application of silica aerogels, the preparation costs must be reduced, and the mechanical properties must be enhanced. Combining aerogels and PUF composites is an attractive approach for achieving these goals as the costs could be reduced and the mechanical properties could be easily enhanced. Therefore, herein, we aim to fabricate composites that simultaneously exhibit the advantages of silica aerogels and SRPUFs. Among various aerogels, PMSQ aerogels using MTMS as a precursor are selected for preparing the composites because they are inherently hydrophobic and flexible and do not require a tedious surface modification step.[29,30] SRPUFs rather than FPUFs or RPUFs are selected for preparing the composites because of their aforementioned inherent thermal conductivities, inherent flexibilities, and open cell structures.[7,11,12,14,31] The fabrication of SRPUF/aerogel composites can be accomplished straightforwardly by pouring the sol state of PMSQ onto SRPUFs. The sol spontaneously permeates the open cells of the SRPUFs, resulting in wet gel SRPUF/aerogel composites that are further dried at ambient pressure to obtain SRPUF/aerogel composites. To maximize the effect of combining the SRPUF and PMSQ aerogel, the optimum composition for synthesizing monolithic PMSQ aerogels with low thermal conductivity is systematically investigated by employing the novel fluoric surfactant FC-4432. This optimum composition is applied to the SRPUF/aerogel composite, and the proper content of PMSQ aerogels is determined. Through the combination of SRPUF and PMSQ aerogel, the SRPUF/aerogel composites with 63 phr (parts per hundred resin) of PMSQ displayed a decline in the thermal conductivity from 41.0 to 36.0 mW/m·K. the sound absorption coefficients of SRPUF/aerogel composite with 45 phr of aerogel increased from 0.57 to 0.67 compared with neat SRPUF at high frequency range. Moreover, the hydrophobicity of the SRPUF/aerogel composites is higher owing to the methyl moieties of the PMSQ aerogels. This simple method can promote the use of aerogels in various industries.

2. Experimental

2.1. Materials

All chemicals used in this study were used as received. Semi-rigid PU foam was provided by Kukdo Chemical Co., Ltd. (South Korea). Methyltrimethoxysilane (MTMS 95%) was purchased from Sigma-Aldrich (USA). Methanol (MeOH, 99.9%) and diethyl ether (DEE) were purchased from Samchun Chemical (South Korea). Oxalic acid solution (CH_2O_4, 0.1 N, reagent grade) was purchased from Acros Organics (USA). Ammonia solution (NH_4OH, 28 wt%) was purchased from Junsei (Japan). FC-4432 (87% polymeric fluorochemical actives, 7% non-fluorochemical actives, and 5% dipropylene glycol monomethyl ether) were purchased from 3M (USA). Distilled water was prepared in-house.

2.2. Preparation of PMSQ aerogel monolith

Before preparing the SRPUF/aerogel composite, several variables were investigated to minimize the thermal conductivity of the PMSQ aerogel. The starting compositions are listed in Table 1. 17 g of MTMS, 48.2 g of MeOH, 8.3 g of water, 12.5 g of CH_2O_4, 6.8 g of 28 wt% NH_4OH were fixed. At the initial composition, besides of NH_4OH solution, starting materials above mentioned were mixed in a glass flask with vigorous stirring. The molar ratio of the starting materials was MTMS:MeOH:water:CH_2O_4=1:12:8.3:0.005. After stirring at room temperature for 10 min, the temperature of the system was increased to 50 ℃ and maintained for 2-20 h to hydrolyze MTMS. Thereafter, 6.8 g of 28 wt% NH_4OH was added to the solution and stirred for 10 min. This solution was transferred to a closed vessel and maintained at 60 ℃ to allow the condensation reaction. The gelation time for all samples was approximately 1.5 h. The samples were then kept in an oven at 60 ℃ for 1 or 2 d to investigate the effect of the aging time, followed by washing with methanol once and exchanging the solvents of the wet gels (mainly MeOH) with DEE, which has a very low surface tension and thus had the potential to decrease the capillary pressure generated when the wet gels were dried three times every 12 h. Finally, the wet gels were dried in an oven at 60 ℃ for 48 h under ambient pressure.

2.3. Preparation of the SRPUF/PMSQ aerogel composite

Figure 1 shows a schematic of the preparation of the SRPUF/PMSQ aerogel composite. Among the compositions investigated in the previous sections, the conditions and molar ratios of the components that afforded the lowest thermal conductivity were considered optimal and were employed in preparing the SRPUF/PMSQ aerogel composites. After hydrolysis under acidic conditions, the sol was poured onto SRPUF. The soaked SRPUF was sealed in a glass tank that was kept airtight at 60 ℃ for 48 h to allow the sol-gel process to proceed in the open cells of SRPUF.

Table 1. Various compositions for optimizing acid-catalyzed hydrolysis reaction and ageing times

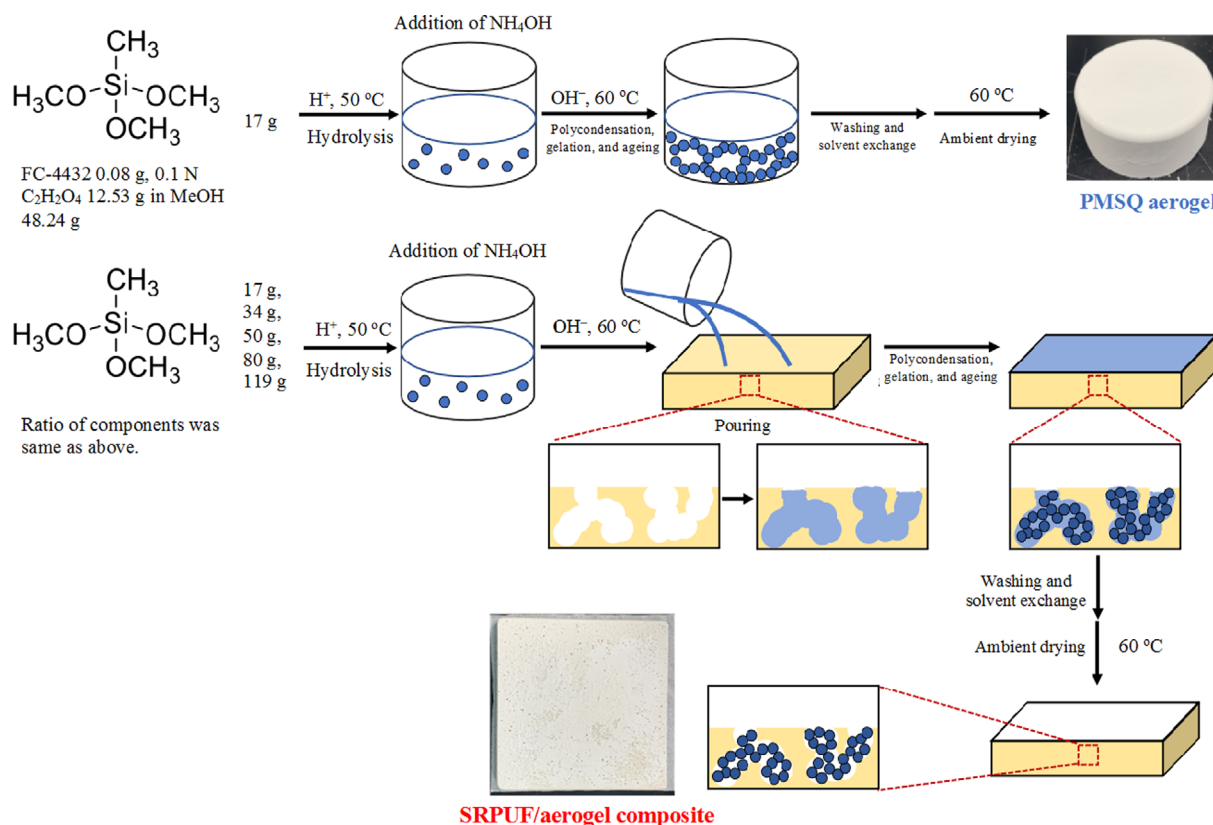| Sample	FC-4432 (g)	Reaction time (h)	Ageing time (h)	Bulk density (kg/m³)	Thermal conductivity (mW/m·K)
AR2	0.08	2	24	-	-
AR10	0.08	10	24	-	-
AR20	0.08	20	24	-	-
AR40	0.08	40	24	-	-
FS0	0.00	20	48	0.982	34.0
FS4	0.04	20	48	0.968	31.5
FS8	0.08	20	48	0.971	28.5

Figure 1. Schematic illustration of preparation of crackless PMSQ aerogels and SRPUF/aerogel composites.

Afterward, the foam was washed with methanol once and the inner solvent (mostly MeOH) was exchanged with DEE three times every 12 h. Finally, the foam was dried at 60 ℃ for 48 h to obtain the SRPUF/PMSQ aerogel composite.

2.4. Characterization

The microstructures of the PMSQ aerogels, SRPUFs, and SRPUF/ PMSQ aerogel composites were investigated by scanning electron microscopy (SEM, Hitachi S-4300, Japan) at an acceleration voltage of 15.0 kV. The bulk density was obtained by measuring the volume and mass of the PMSQ aerogel, SRPUF, and SRPUF/ PMSQ. The thermal conductivity was measured using a transient heat flow meter (HFM 436 Lambda, Netzsch GmbH, Germany). To measure the sound absorption coefficient, two impedance tube devices were used for low (SW420, BSWA, China) and high (SW470, BSWA, China) frequencies, with two 1/4-inch microphones (MPA416, BSWA, China). Contact angle of water was measured with Phoenix-MT(M) (SEO, Korea). Compression tests were performed on a monolithic cylindrical sample using a Universal Testing System (DaeKyung, China). The neat SRPUF, SRPUF/aerogel composites, and PMSQ aerogel were placed between the testing plates and was compressed at a speed of 2 mm/min to 60%, 80% strain respectively (PMSQ aerogel was 60% and neat SRPUF, SRPUF/aerogel composites were 80%). Thermal properties of samples were investigated by thermogravimetric analysis (TGA) using a TGA N-1000 (SCINCO, Korea) at a heating rate of 10 ℃ under nitrogen flow.

3. Results and discussion

3.1. Effects of acid-catalyzed reaction and ageing times

PMSQ aerogel monoliths were prepared by controlling several synthesis parameters without changing the amount of surfactant FC-4432, which was fixed at 0.08 g. The parameters used in synthesizing each aerogel sample are listed in Table 1. Figure 2
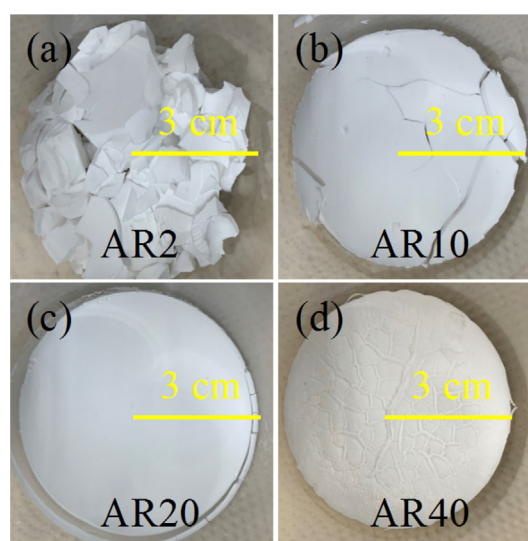

Figure 2. Photographic images of PMSQ aerogels prepared by varying the acid-catalyzed hydrolysis reaction time: (a) 2 h, (b) 10 h, (c) 20 h, and (d) 40 h.

shows images of the PMSQ aerogel monoliths synthesized by varying the acid-catalyzed hydrolysis reaction time (2, 10, 20, and 40 h). Figures 2(a) and (b) show significant cracking in the aerogels after drying at ambient pressure. Samples prepared with the short period of the acid catalyzed reaction (2 and 10 h) cracked after complete drying (Figure 2(a) and (b)), whereas samples prepared with the long period of the acid catalyzed reaction (20 and 40 h) dried without cracks (Figure 2(c) and (d)). Cracks in AR2 and AR10 engendered during the drying process were caused by the thin structures. As shown in Figure 3, AR2 and AR10 had thinner network structures than AR20 and AR40. This indicates the presence of few unreacted silanol groups and that the network structure was strengthened when the reaction time for the acid-catalyzed hydrolysis was extended beyond 20 h. However, AR40 had inferior mechanical properties and was powdery because of aggregation of the particles (as shown in Figures 2(d) and 3(d)).

Figure 3 depicts SEM microphotographs of the samples shown in Figure 2. As the reaction time for the acid-catalyzed hydrolysis increased, particle aggregation became more severe. AR2 had a uniform and stable structure (Figure 3(a)). However, for the short reaction period, cracks occurred owing to the unreacted silanol groups. Figures 3(b)-(d) shows that a longer hydroly-
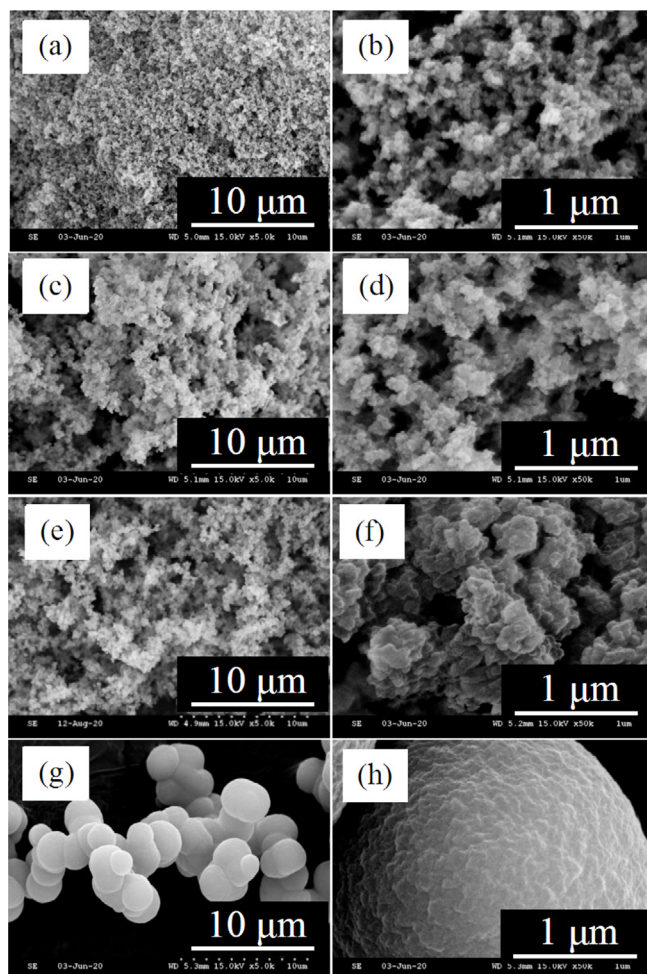
sis time produced larger particles. On this basis, the optimum time for the acid-catalyzed reaction was 20 h. After determining the optimum time for the acid-catalyzed hydrolysis reaction, the optimum time for ageing was investigated. Compared with the AR20 sample synthesized by 24 h ageing, the FS8 sample (Figure 4(c)) synthesized by 48 h ageing had a smoother surface texture. From these results, the optimum ageing time was 48 h.

3.2. Effects of fluoric surfactant FC-4432

One of the crucial issues in the sol-gel production of aerogels is suppressing phase separation, which induces the formation of irregular and large particles and pore sizes. In previous studies, various cationic surfactants such as cetyltrimethylammonium chloride and cetyltrimethylammonium bromide were used to suppress the phase separations.[30,32-37] However, a large amount of surfactant is needed in the synthesis of aerogels, where the residue persists as impurities in the aerogels. In contrast, only a small amount of FC-4432, a fluorocarbon-based surfactant, is needed to lower the surface tension and improve the wettability of materials. Despite the interesting properties of fluorocarbon-based surfactants, few studies have used fluorocarbon-based surfactants in the synthesis of aerogel monoliths. Therefore, in this study, the effects of the fluorocarbon-based surfactant were investigated by adding surfactant FC-4432 to the PMSQ aerogel, and the optimum loading of FC-4432 was determined empirically. To investigate the effects of FC-4432 on the PMSQ aerogels, other synthesis parameters (the temperature and time of the acid-step, base-step, aging, and drying, as well as the molar ratio of MTMS:MeOH:water:CH_2O_4:NH_4OH) were fixed while varying the amount of surfactant (FC-4432).

Figure 4 shows images of the three PMSQ aerogel monoliths prepared with different amounts of the surfactant FC-4432. Because the reaction period was adequate, no cracks or shrinkages appeared in any of the samples. Figure 4 indicates that when more FC-4432 was added, the aerogel monoliths became
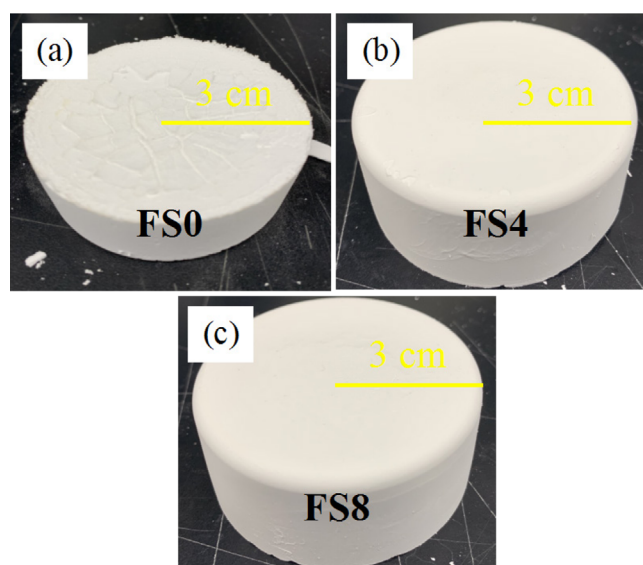

Figure 3. SEM microphotographs of PMSQ aerogel prepared by varying the acid-catalyzed hydrolysis reaction time: (a), (b) 2 h, (c), (d) 10 h, (e), (f) 20 h, and (g), (h) 40 h.

Figure 4. Photographs of PMSQ aerogel with different amounts of surfactant FC-4432: (a) 0 g, (b) 0.04 g, and (c) 0.08 g.
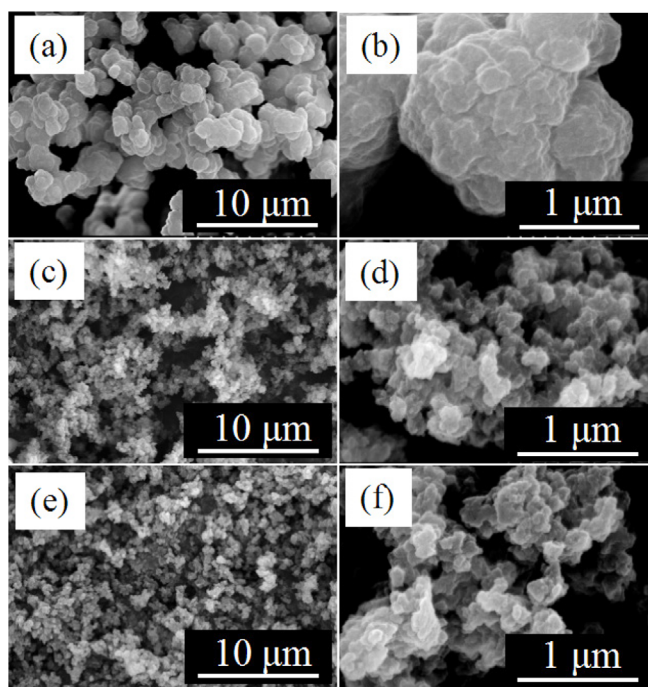
Figure 5. SEM microphotographs of PMSQ aerogel with different amounts of surfactant FC-4432: (a), (b) 0 g, (c), (d) 0.04 g, and (e), (f) 0.08 g.

smoother and FS0 prepared without the addition of FC-4432 had a powdery texture (Figure 4(a)). Figure 5 shows SEM microphotographs of FS0, FS4 (prepared with 0.04 g of FC-4432), and FS8 (prepared with 0.08 g of FC-4432). With increasing loading of the surfactant FC-4432, the particle size became smaller. FS0 exhibited the largest particles and pores, where the powdery texture of FS0 originated from the large particle size (Figure 4(a), Figure 5(a)). FS4 comprised smaller particles with smaller pore sizes than FS0 (Figures 5(a) and (b)). FS8 had the smallest particle and pore sizes (Figure 5(c)). With increasing loading of FC-4432, the particle and pore sizes decreased. These results show that FC-4432 efficiently suppressed phase separation during the sol-gel process when added in small quantities.

3.3. Thermal conductivity of PMSQ aerogels

The thermal conductivity of the three samples, FS0, FS4, and FS8, was investigated using a heat-flow meter. Generally, the thermal conductivity of a porous material is the sum of the gas (λ_g), solid (λ_s), and radiation (λ_r) thermal conductivities (Eq. (1)).[34,38-41]

$$\lambda_t = \lambda_g + \lambda_s + \lambda_r \tag{1}$$

Among these components, the low thermal conductivity of the aerogel mainly originates from low λ_g and λ_s. The λ_s of the monolithic aerogels strongly depended on the bulk density. The high λ_s originates from the very high porosity (90-98%), which lowers the bulk density of the aerogels. This contribution to the thermal conductivity scales with the aerogel density (ρ), as shown in Eq. (2).[42,43]

$$\lambda_s \approx \rho^\lambda \text{ with } \lambda = 1.2 - 1.8 \tag{2}$$
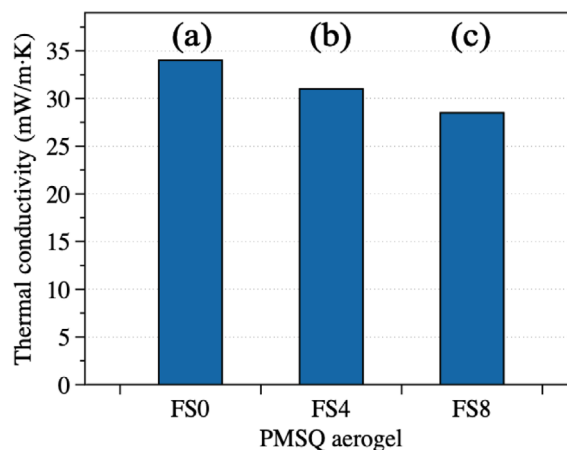

Figure 6. Thermal conductivities of PMSQ aerogel with different amounts of surfactant FC-4432: (a) 0 g, (b) 0.04 g, and (c) 0.08 g.

Figure 6 shows the thermal conductivities of the three samples (FS0, FS4, and FS8). The thermal conductivities of the three samples decreased proportionally with the amount of surfactant FC-4432. However, the densities and porosities of the three samples were significantly different (Table 1). Thus, it is reasonable that the differences in the thermal conductivity resulted from differences in λ_g. If gas such as air permeates into the pores of the aerogels, λ_g increases because of the gas conductivity, as shown in Eq. (3):[34,40]

$$\lambda_g = \frac{\lambda_{g,0}\phi}{1 + 2\beta K_n} \tag{3}$$

where ϕ is the porosity and $\lambda_{g,0}$ is the conductivity of free gas. β is a constant that includes the interaction between the gas molecules and the pore walls, and K_n is the Knudsen number, as shown in Eq. (4):

$$K_n = l_g/D \tag{4}$$

where l_g is the mean free path of the gas molecules, and D is the pore diameter. Therefore, the gas thermal conductivity of the aerogels decreased when the pore diameter was reduced. It is difficult to determine the pore diameter of PMSQ aerogels using porosimetry techniques, such as nitrogen absorption-desorption, because of the flexibility of these materials under compressive stress. However, the pore diameters of these samples (FS0, FS4, and FS8) could be estimated from the SEM microphotographs (Figure 5). As shown in Figure 5, FS8 seemed to have the smallest pore diameters (Figure 5(c)), and FS0 seemed to have the largest pore diameters (Figure 5(a)). This accounts for the differences in the thermal conductivity.

3.4. Preparation of SRPUF/aerogel composites

From the above experimental data, the optimum parameters for synthesizing crackless aerogels with the lowest thermal conductivity were determined and were applied in the preparation of SRPUF/aerogel composites. After acid-catalyzed hydrolysis for 20 h, NH$_4$OH was added to the solution to promote condensation, causing gelation. After 5 min, the sol was poured onto the SRPUFs. The rest of the processes were almost the same as in
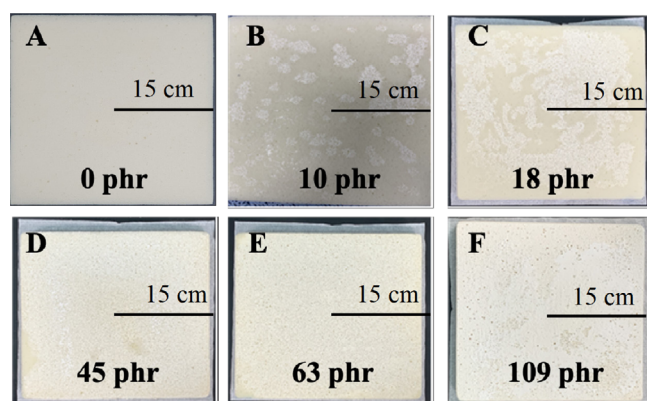
Figure 7. Surface images of SRPUF/aerogel composites with different amounts of PMSQ aerogel: (A) 0 phr, (B) 10 phr, (C) 18 phr, (D) 45 phr, (E) 63 phr, and (F) 109 phr.

preparation of the aerogels: gelation and ageing at 60 ℃ for 48 h, solvent exchange with DEE, and drying at 60 ℃. In this study, five SRPUF/aerogel composite samples were prepared using different amounts of PMSQ aerogels to investigate the effect of the aerogels on the SRPUFs. Figure 7 shows the images of the
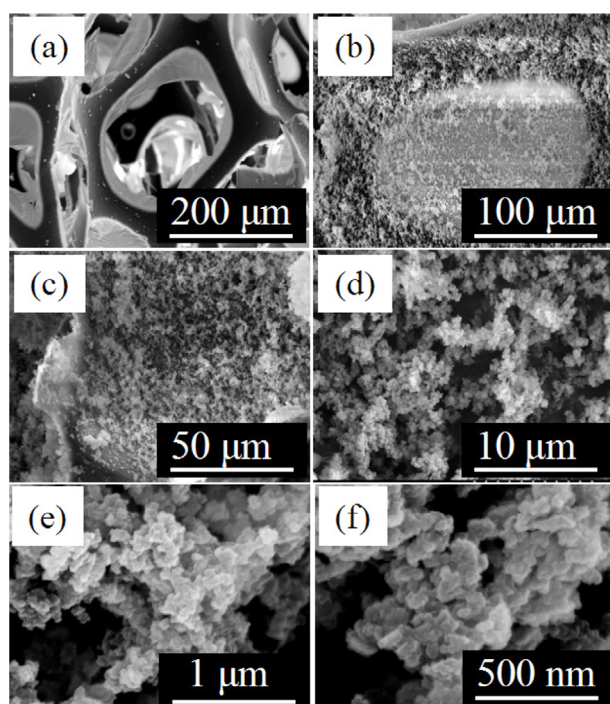

Figure 8. SEM microphotographs of (a) neat SRPUF and (b–f) SRPUF/aerogel composites (PUFA45).

SRPUF/aerogel composites. The aerogel content in the SRPUF by weight was determined in phr units 45 phr of aerogel is the minimum amount required to cover the entire surface of the SRPUFs (Figures 7(a)-(d)). Figure 8 shows SEM microphotographs of the neat SRPUF and SRPUF/aerogel composites. Figure 8(a) depicts the structure of neat SRPUF, and Figures 8(b)-(d) shows the structure of PUFA45. These SEM microphotographs demonstrate that PMSQ aerogels were successfully synthesized in the open cells of the SRPUFs. The pearl necklace-like structure is shown in Figures 8(b)-(d). The densities of the neat SRPUF and SRPUF/aerogel composites are listed in Table 2. When more aerogel was added, the density of the composite increased from 18.75 to 39.19 kg/m³. Uniaxial compression test was conducted to investigate the change of elastic property of SRPUF, SRPUF/aerogel composites, and PMSQ aerogel. The stress-strain curves for samples of this study are shown in Figure S1. The initial linear region at about 0-4% corresponds to the elastic behavior. The plateau is a region of densification, which starts at over 65% deformation with a sharp increase of stress as a function of compression ratio. In this region, the cell structures approached each other to the degree of making physical contact with each other, hence the sharp increase in stress at these deformations. The shapes of the stress-strain curves are similar for SRPUF and SRPUF/aerogel composites in this study. The absolute values of the plateau stresses and Young's modulus were varied independent on the content of aerogels, but the general appearances of the curves are the same. The Young's modulus of neat SRPUF, PUFA45, PUFA63, and PUFA109 was 7.0, 6.9, 8.8, and 5.2 kPa respectively. Thermal stability of SRPUF/aerogel composites was superior to neat SRPUF (Figure S2). While thermal decomposition of neat SRPUF occurred over 151 ℃, thermal decomposition of all SRPUF/aerogel composites started over 210 ℃ independent on the content of PMSQ aerogel.

3.5. Thermal conductivity of SRPUF/aerogel composites

The thermal conductivities of the five SRPUF/aerogel composites were measured using a heat-flow meter. Figure 9 shows that the thermal conductivities of these samples decreased with increasing amounts of aerogel. The thermal conductivities of the neat SRPUF, PUFA10, PUFA18, PUFA45, PUFA63, and PUFA109 were 41.0, 40.4, 39.1, 36.3, 36.0, and 36.1 mW/m·K, respectively. Though the densities of the composites increased in proportion to the increase in the aerogel content, there was an obvious decrease in the thermal conductivity. These results suggest that the gas thermal conductivity decreased (Eq. (2)). Because the open cells of the SRPUFs were filled with aerogels, large pores (~1 μm)

Table 2. Bulk densities, thermal conductivities, and sound absorption coefficients of SRPUF/aerogel composites

Sample	Bulk density (kg/m³)	Thermal conductivity (mW/m·K)	Sound absorption coefficient[a]
Neat SRPUF	18.75	41.0	0.57
PUFA10	20.63	40.4	0.56
PUFA18	22.13	39.1	0.61
PUFA45	27.19	36.3	0.67
PUFA63	30.56	36.0	0.64
PUFA109	39.19	36.1	0.62

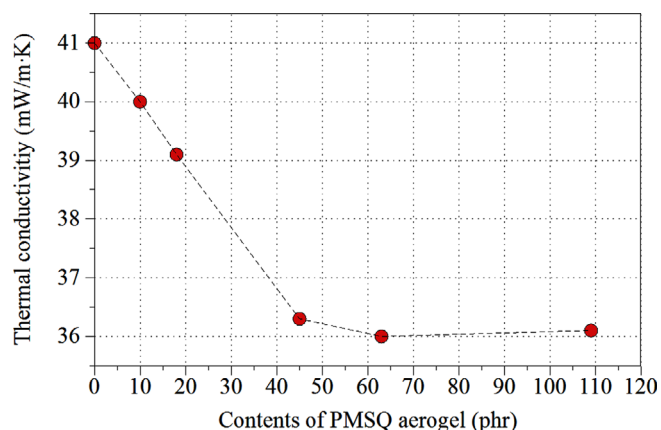[a]Average values of sound absorption coefficients at higher range frequency.

Figure 9. Thermal conductivities of neat SRPUF and SRPUF/aerogel composites with respect to the amount of PMSQ aerogel.

were converted to the mesopores of the aerogels. Consequently, the gas thermal conductivity would be reduced. In summary, the thermal conductivity of the SRPUF/aerogel composites was controlled by two effects. One is a decreasing effect, and the other is an increasing effect. The decreasing effect is associated with reduction of the gas thermal conductivity caused by narrowing of the pore diameter because the larger pores of the neat SRPUF were substituted by smaller pores in the PMSQ aerogels. The increasing effect is associated with the increase in the solid thermal conductivity. Before adding the aerogels, the open cells of the SRPUF contained air or gas. After addition of the aerogels, air was displaced by the PMSQ aerogels, resulting in an increase in density. Consequently, the solid thermal conductivity increased. For these reasons, when the aerogel plays a filler-

like role in thermal insulation materials, it is important to determine the optimum content. In this study, the sample with 63 phr of aerogel had the lowest thermal conductivity (lower than that of the sample with 109 phr of aerogel added).

3.6. Sound insulating ability and hydrophobicity

Generally, SRPUFs have better sound absorption ability than RPUFs because the sound absorption properties originate from the open cells and flexibility.[44,45] Since PMSQ aerogels prepared by using MTMS as a precursor have a flexible 3D network and mesoporous structures, the PMSQ aerogels exhibit a high sound absorption coefficient, especially in higher frequency range.[46] To compare the sound absorption ability of neat SRPUF and the SRPUF/aerogel composite, the range of sound absorption coefficients of all samples were divided into two area (mid frequency range and higher frequency range). Figure 10(a) shows the sound absorption coefficients of neat SRPUF and SRPUF/aerogel composites at the frequencies of 0.4-5.0 kHz, and Figure 10(b) and (c) show the sound absorption coefficients at the frequencies of 0.5-2.5 kHz (mid frequency range) and at the frequencies of 2.5-5.0 kHz (higher frequency range), respectively. Figure 10(d)-(f) show average sound frequency coefficients obtained by calculation arithmetic mean of absorption coefficients at the frequencies of 0.5-2.5 kHz (Figure 10(d)), 0.5-2.5 kHz (Figure 10(e)), and 2.5-5.0 kHz (Figure 10(f)). Sound absorption coefficients of all samples increased until 1.5 kHz, and they decreased at more than 1.5 kHz. Among them, PUFA10 exhibited a singular behavior compared to the other SRPUF/aerogel composites (Figure 11(a)). This can be attributed to the poor coverage of PMSQ aerogels in PUFA10 as shown in Figure 7. Except PUFA10, SRPUF/aerogel composites showed
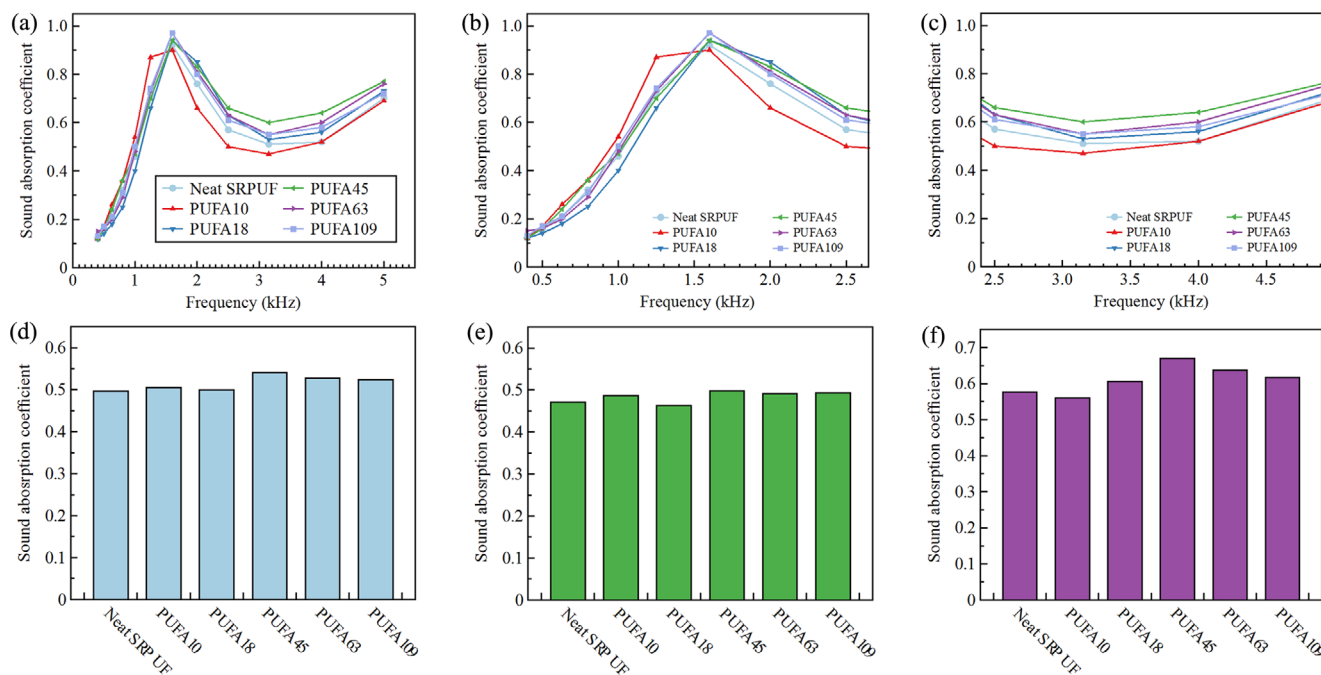

Figure 10. Sound absorption coefficients of neat SRPUF and SRPUF/aerogel composites. (a) Sound absorption coefficients from 0.4 kHz to 5.0 kHz (all range frequency), (b) from 0.5 kHz to 2.5 kHz (mid-range frequency), (c) from 2.5 kHz to 5.0 kHz. Average sound absorption coefficients of the neat SRPUF and SRPUF/aerogel composites (higher range frequency). (d) average sound absorption coefficients from 0.4 kHz to 5.0 kHz, (e) from 0.5 kHz to 2.5 kHz, and (f) from 2.5 kHz to 5.0 kHz.
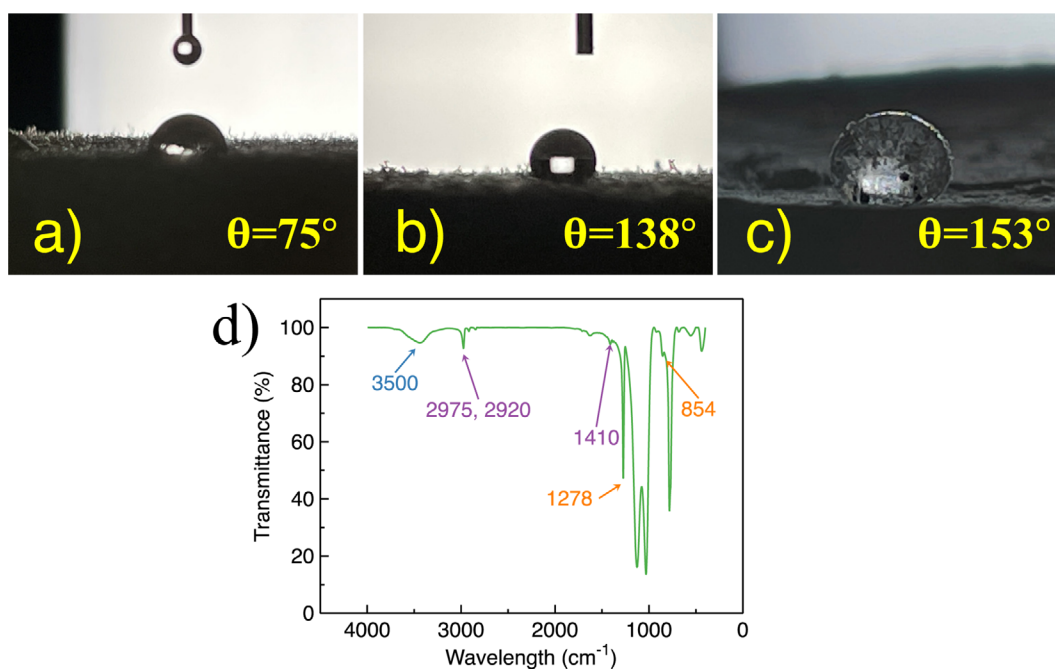
Figure 11. Water contact angles of (a) neat SRPUF, (b) SRPUF/aerogel composite, and (c) SRPUF/PMSQ aerogel composite. FT-IR spectrum of the PMSQ aerogel (FS8) (d).

better sound absorption coefficients than the neat SRPUF in more than 1.5 kHz. These trends could be clearly observed in Figure 10(c) and (f). With increasing the loading amount of PMSQ aerogels to 45 phr, sound absorption coefficients increase at higher frequency range owing to increased densities and decreased pore sizes. However, more than 45 phr of aerogel overfills the pores, which interferes with sound wave propagation. As a result, sound absorption coefficient decreases above 45 phr. Therefore, to achieve better sound absorption coefficient in higher frequency range, 45 phr of aerogel would be an optimum loading. The SRPUF/aerogel composite afforded a lower thermal conductivity, as well as improved sound absorption coefficients in higher frequency range compared to neat SRPUF.

In various applications such as building interior materials and automobiles, hydrophobicity was vital to maintain the structure of materials against moistures. PMSQ aerogels generally have high hydrophobicity owing to few hydroxy groups, abundant methyl moieties, and nanoscale roughness.[47,48] Chemical composition of the PMSQ aerogel used in this work (FS8) was confirmed using FT-IR. Figure 11(d) shows the FT-IR spectrum of the PMSQ aerogels in the region of 4000-400 cm^{-1}. From the FT-IR spectrum, abundant methyl groups and few hydroxy groups of the PMSQ aerogel were verified. The small peak at 3600-3400 cm^{-1} demonstrates few hydroxy groups. The peaks at 2975, 2920, and 1410 cm^{-1} are characteristic peaks of stretching, bending, and deformation vibration of C-H bonds in methyl group, respectively. The peaks at 1278 and 854 cm^{-1} indicate the bending and stretching vibration of methyl groups in Si-CH$_3$, respectively.[49,50] Figure 11 shows water contact angles of neat SRPUF (a), SRPUF/aerogel composite (PUFA45, (b)), and PMSQ aerogel (c). As shown in Figure 11, water contact angle of the SRPUF/aerogel increased from 75 to 138° because open cells at the SRPUF surface were filled with hydrophobic PMSQ aerogel.

4. Conclusions

In summary, we demonstrated a SRPUF/aerogel composite with improved thermal insulating ability and sound insulating ability compared with neat SRPUF. The SRPUF/aerogel composite was prepared by optimizing the composition of the monolithic PMSQ aerogel by controlling critical factors, including the temperature, time, and composition and by employing the novel fluoric surfactant FC-4432, which effectively suppressed phase separation of the PMSQ aerogel. The effect of surfactant FC-4432 on the phase separation was studied further. Compared with FS0 (PMSQ aerogel monolith without surfactant FC-4432), FS8 (PMSQ aerogel monolith with 0.08 g of surfactant FC-4432) had a smaller particle size and had lower thermal conductivity (28.5 mW/m·K). In preparing the SRPUF/aerogel composites using the optimum composition for the PMSQ aerogel, the sol state of PMSQ was poured onto the surface of the SRPUFs, followed by gelation of PMSQ on the SRPUFs. To investigate the effect of combining the PMSQ aerogel and SRPUFs, PMSQ aerogels at different loadings (10-109 phr) were poured onto the SRPUFs, where 45 phr of aerogels is the minimum amount required to cover the entire surface of the SRPUFs. The thermal conductivity of neat SRPUF was 41.0 mW/m·K and the sound absorption coefficient at higher frequency range of neat SRPUF was 0.57. With increased loading of the PMSQ aerogel, the thermal conductivity of the SRPUF/aerogel composite decreased and reached a value of 36.0 mW/m·K for PUFA63. At higher frequency range, the sound absorption coefficients of SRPUF/aerogel composite with 45 phr of aerogel increased from 0.57 to 0.67. The integrated SRPUF/aerogel composites achieved lower thermal conductivities without sacrificing the inherent sound absorption properties of SRPUFs, and even exhibited higher hydrophobicity. Therefore, we believe that this strategy will provide an avenue for the industrial applica-

tion of PMSQ aerogels and SRPUFs as heat and sound insulation materials.

Supporting information: Information is available for compression tests and TGA thermograms of PMSQ aerogel, neat SRPUF, and SRPUF/aerogel composites. The materials are available *via* the Internet at http://www.springer.com/13233.

References

(1) F. Ardente, M. Beccali, M. Cellura, and M. Mistretta, *Energy Build.*, **40**, 1 (2008).
(2) R. Choudhary, *Build. Environ.*, **51**, 243 (2012).
(3) Y.-S. Jeong, S.-E. Lee, and J.-H. Huh, *Energy Build.*, **49**, 437 (2012).
(4) C. Ji, T. Hong, and H. S. Park, *Energy Build.*, **72**, 186 (2014).
(5) U. Y. A. Tettey, A. Dodoo, and L. Gustavsson, *Energy Build.*, **82**, 369 (2014).
(6) H. Abbasi, M. Antunes, and J. I. Velasco, *Eur. Polym. J.*, **69**, 273 (2015).
(7) E. Linul, C. Vălean, and P.-A. Linul, *Polymers*, **10**, 1298 (2018).
(8) M. Antunes, G. Gedler, and H. Abbasi, J. I. Velasco, *Mater. Today: Proc.*, **3**, S233, (2016).
(9) S. Demirel and B. E. Tuna, *Polym. Test*, **76**, 146 (2019).
(10) G. Yang, X. Liu, and V. Lipik, *J. Mater. Sci.*, **53**, 9463 (2018).
(11) R. Verdejo, R. Stämpfli, M. Alvarez-Lainez, S. Mourad, M. Rodriguez-Perez, P. Brühwiler, and M. Shaffer, *Compos. Sci. Technol.*, **69**, 1564 (2009).
(12) E. Ciecierska, M. Jurczyk-Kowalska, P. Bazarnik, M. Gloc, M. Kulesza, M. Kowalski, S. Krauze, and M. Lewandowska, *Compos. Struct.*, **140**, 67 (2016).
(13) M. Thirumal, D. Khastgir, N. K. Singha, B. Manjunath, and Y. Naik, *J. Appl. Polym. Sci.*, **108**, 1810 (2008).
(14) N. V. Gama, A. Ferreira, and A. Barros-Timmons, *Materials*, **11**, 1841 (2018).
(15) M. Schmidt and F. Schwertfeger, *J. Non-Cryst. Solids*, **225**, 364 (1998).
(16) A. S. Dorcheh, and M. Abbasi, *J. Mater. Process. Technol.*, **199**, 10 (2008).
(17) S. Henning and L. Svensson, *Phys. Scr.*, **23**, 697 (1981).
(18) E. Cohen and L. Glicksman, *J. Heat Transfer*, **137** (2015).
(19) E. Frackowiak and F. Beguin, *Carbon*, **39**, 937 (2001).
(20) G. Pajonk, *Appl. Catal.*, **72**, 217 (1991).
(21) W. Volksen, R. D. Miller, and G. Dubois, *Chem. Rev.*, **110**, 56 (2010).
(22) A. Fidalgo, M. E. Rosa, and L. M. Ilharco, *Chem. Mater.*, **15**, 2186 (2003).
(23) B. M. Novak, D. Auerbach, and C. Verrier, *Chem. Mater.*, **6**, 282 (1994).
(24) N. Leventis, C. Sotiriou-Leventis, G. Zhang, and A.-M. M. Rawashdeh, *Nano Lett.*, **2**, 957 (2002).
(25) M. Meador and E. Fabrizio, *Chem. Mater.*, **17**, 1085 (2005).
(26) V. D. Land, T. M. Harris, and J. M. Henshaw, *J. Non-Cryst. Solids*, **316**, 238 (2003).
(27) D. M. Smith, D. Stein, J. M. Anderson, and W. Ackerman, *J. Non-Cryst. Solids*, **186**, 104 (1995).
(28) S. S. Prakash, C. J. Brinker, A. J. Hurd, and S. M. Rao, *Nature*, **374**, 439 (1995).
(29) K. Kanamori, M. Aizawa, K. Nakanishi, and T. Hanada, *Adv. Mater.*, **19**, 1589 (2007).
(30) G. Hayase, K. Kanamori, and K. Nakanishi, *Microporous Mesoporous Mat.*, **158**, 247 (2012).
(31) N. Marcovich, M. Kurańska, A. Prociak, E. Malewska, and K. Kulpa, *Ind. Crop. Prod.*, **102**, 88 (2017).
(32) Y. Zhang, J. Wang, and X. Zhang, *J. Colloid Interface Sci.*, **515**, 1 (2018).
(33) G. Hayase, K. Kanamori, A. Maeno, H. Kaji, and K. Nakanishi, *J. Non-Cryst. Solids*, **434**, 115 (2016).
(34) G. Hayase, K. Kugimiya, M. Ogawa, Y. Kodera, K. Kanamori, and K. Nakanishi, *J. Mater. Chem. A*, **2**, 6525 (2014).
(35) M. Kurahashi, K. Kanamori, K. Takeda, H. Kaji, and K. Nakanishi, *RSC Adv.*, **2**, 7166 (2012).
(36) K. Kanamori, K. Nakanishi, and T. Hanada, *J. Ceram. Soc. Jpn.*, **117**, 1333 (2009).
(37) J. P. Vareda, P. Maximiano, L. P. Cunha, A. F. Ferreira, P. N. Simões, and L. Durães, *J. Colloid Interface Sci.*, **512**, 64 (2018).
(38) R. Baetens, B. P. Jelle, and A. Gustavsen, *Energy Build.*, **43**, 761 (2011).
(39) K. Kanamori and K. Nakanishi, *Chem. Soc. Rev.*, **40**, 754 (2011).
(40) X. Lu, M. Arduini-Schuster, J. Kuhn, O. Nilsson, J. Fricke, and R. Pekala, *Science*, **255**, 971 (1992).
(41) G. Wei, Y. Liu, X. Zhang, F. Yu, and X. Du, Int. *J. Heat Mass Transf.*, **54**, 2355 (2011).
(42) A. C. Pierre and G. M. Pajonk, *Chem. Rev.*, **102**, 4243 (2002).
(43) T. Burger and J. Fricke, *Für. Phys. Chem.*, **102**, 1523 (1998).
(44) A.E. Tiuc, O. Vasile, and H. Vermesan, *Rom. J. Acoust. Vib.*, **12**, 111 (2015).
(45) A.E. Tiuc, O. Vasile, and H. Vermesan, and P. M. Andrei, *Mater. Plast.*, **55**, 419 (2018).
(46) X. Li, Z. Yang, K. Li, S. Zhao, Z. Fei, and Z. Zhang, *J. Sol-Gel Sci. Technol.*, **92**, 652 (2019).
(47) J. Ding, K. Zhong, S. Liu, X. Wu, X. Shen, S. Cui, and X. Chen, *Powder Technol.*, **373**, 716 (2020).
(48) X. Wu, K. Zhong, J. Ding, X. Shen, S. Cui, Y. Zhong, and J. Ma, X. Chen, *J. Non-Cryst. Solids*, **530**, 119826 (2020).
(49) A. V. Rao, S. S. Latthe, C. Kappenstein, V. Ganesan, M. C. Rath, and S. N. Sawant, *Appl. Surf. Sci.*, **257**, 3027 (2011).
(50) F. Wang, X. Wang, A. Xie, Y. Shen, W. Duan, Y. Zhang, and J. Li, *Appl. Phys. A-Mater. Sci. Process.*, **106**, 229 (2012).